Title

Crystalline poly(triazine imide) based g-CN as an efficient electrocatalyst for counter electrodes of dye-sensitized solar cells using a triiodide/iodide redox electrolyte

Journal

Journal of Materials Chemistry A, 3(48)

ISSN

2050-7488

Authors

Lee, Woo-ram
Jun, Young-Si
Park, Jihee
et al.

Publication Date

2015

DOI

10.1039/c5ta08650g

COMMUNICATION

Crystalline poly(triazine imide) as an efficient electrocatalyst for counter electrodes of dye-sensitized solar cells using a triiodide/iodide redox electrolyte

Received 00th January 20xx,
Accepted 00th January 20xx

DOI: 10.1039/x0xx00000x

Woo-ram Lee, Young-Si Jun, Jihee Park, and Galen D. Stucky*

We report utilization of graphitic carbon nitride (g-CN) as an electrocatalyst for dye-sensitized solar cells (DSSCs). Crystalline poly(triazine imide) based g-CN was synthesized via a modified ionothermal method, and deposited onto the counter electrodes along with a conductive additive and a sacrificial polymer binder. The resulting DSSCs exhibited a power conversion efficiency (7.8%) comparable to that of conventional Pt catalyst (7.9%), confirming the excellent catalytic activity of poly(triazine imide) g-CN as a non-precious metal electrocatalyst.

Dye-sensitized solar cells (DSSCs) have been considered a promising alternative to conventional silicon solar cells due to their low cost, easy fabrication, and high performance.[1,2] The counter electrode (CE, cathode), which is used to collect the electrons from the external circuit and to catalyze the reduction of the redox couple in electrolytes in DSSCs, usually consists of a fluorine-doped tin oxide (FTO) glass coated with a catalyst. Platinum is the most widely used CE catalyst owing to its superior electrical conductivity and catalytic activity, but the high cost of this metal hinders its use for the industrial mass production of DSSCs.[3] Several types of new materials such as inorganic materials, polymers, carbon materials, multiple compounds, and composites have been proposed as alternative electrocatalysts.[3–6]

Carbon-based materials, including carbon nanotubes, graphenes, and mesoporous graphitic carbons, are of particular interest as metal-free CE catalysts.[7,8] They are inexpensive, abundant, non-toxic, and conductive, meeting most of requirements for commercial electrode materials. Furthermore, they are easily processable into a shape and composition favorable for target applications.[9] For example, incorporation of heteroatoms, especially O,[10] N,[11] and halogens,[12] creates more redox-active sites and increases surface hydrophilicity, thereby improving the electrocatalytic activity of pristine carbon materials in the triiodide reduction of DSSCs. Changes in the sp^2 hybridized carbon structure, resulting from the introduction of heteroatoms, significantly alters the DSSC physicochemical and electronic properties. A fundamental understanding of the structure/composition/function relationships is, therefore, crucial for the discovery and design of more efficient CE electrocatalysts based on carbon materials. For this purpose, novel synthetic approaches are needed for the design of efficient heteroatom configured carbon-based electrocatalysts.

Graphitic carbon nitride (g-CN) is an organic compound that consists of alternating sp^2 hybridized carbon and nitrogen atoms.[13] Analogous to graphitic carbon materials, this organic polymer features controllable surface termination, i.e. curvatures, edges and heteroatom dopants favorable for substrate adsorption/desorption and electron relocalization/transfer, as well as controllable electronic band structure.[14] Its intrinsic semiconducting property coupled with its electron-rich nitrogen surface functionality imparts excellent electro-, organo- and photo-catalytic activities in a number of catalytic applications, such as Friedel-Crafts,[15] CO_2 activation,[16] oxygen reduction/evolution[17,18] and hydrogen evolution reactions,[19,20] thereby rendering g-CN a promising candidate for enabling more efficient conversion chemistries. For example, optimally structured g-CN showed 90% conversion efficiency in the Friedel-Crafts acylation of benzene while the efficiency of graphite was only 1%.[15] In spite of such desirable properties, to the best of our knowledge, g-CN has not been employed as a CE catalyst in DSSCs, possibly due to its poor electrical conductivity.[18] In order to resolve this issue, two additive materials are used in this research, along with g-CN, in the synthesis and processing of the CE film used in this study. For the formation of g-CN, crystalline poly(triazine imide) (cPTI) is chosen because of its (electro-)chemical stability and well-defined structure and composition.[21–23] Ionothermal syntheses using inert molten salt and heteroatom containing precursors lead to the bulk formation of a cPTI that is homogeneously intercalated by alkali metal halides; and, also incorporated with other types of heteroatoms by the replacement of trigonal N atoms. In addition this synthesis strategy facilitates charge transfer and adsorbate adsorption/desorption. Furthermore, this 'born-in-halogen' nature is expected to endow the cPTI with compatibility for I^-/I_3^- electrolyte chemistry, in contrast to the catalyst corrosion by the electrolyte that occurs when the traditional Pt is used.[24,25] The resulting DSSCs with the cPTI CE show high power conversion efficiency (*PCE*), comparable to that of DSSCs with a conventional Pt CE.

[a] *Department of Chemistry and Biochemistry, University of California, Santa Barbara, CA 93106, USA. E-mail: stucky@chem.ucsb.edu*
[b] *W.-r. Lee and Y.-S. Jun contributed equally to this work.*
† Electronic Supplementary Information (ESI) available: Experimental details, characterization of cPTI-MCA-LiKCl-550 and photovoltaic performance data.

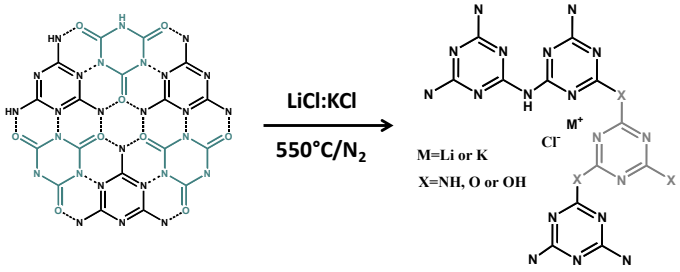

Scheme 1. Ionothermal synthesis of cPTI using MCA as a precursor.

cPTI was prepared via a modified ionothermal synthesis method.[22] A melamine-cyanuric acid (MCA) complex was used as a pre-organized, nitrogen-rich and oxygen-containing molecular precursor.[26] The goal is to homogeneously incorporate O into the cPTI framework, in order to create additional redox active sites for triiodide reduction (Scheme 1).[21,27] Thermal polycondensation of MCA in an eutectic mixture of LiCl:KCl (45:55 wt%) at 550 °C under nitrogen in an open glass container yields a pale yellow powder after removal of the excess salt. It is referred to as cPTI-MCA-LiKCl-550 since nitrogen-rich molecular precursors including melamine or dicyandiamide (DCDA) generate cPTI intercalated with Li, K and Cl at 550~600 °C.[22,28]

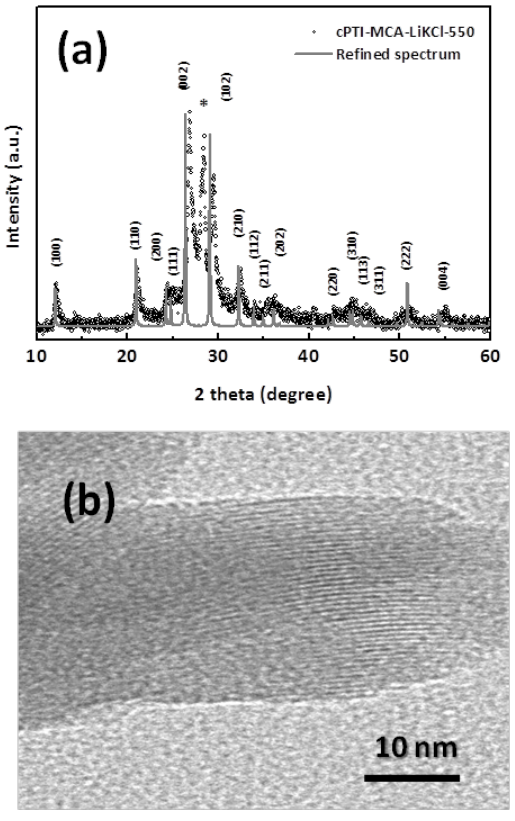

Figure 1. (a) PXRD pattern with refined spectrum and (b) TEM image of cPTI-MCA-LiKCl-550.

Powder X-ray diffraction (PXRD) patterns of cPTI-MCA-LiKCl-550 show well-resolved and intense peaks of a crystalline phase, while PTI prepared from DCDA exhibits no crystallinity at 550 °C, nor do samples prepared in the presence of heteroatom containing molecular precursors such as 4-amino-2,6-dihydroxypyrimidine (4-AP) or 2,4,6-triaminopyrimidine (TAPI) (Figure 1a).[21,28] The diffraction pattern of cPTI-MCA-LiKCl-550 is in good agreement with that of cPTI-DCDA-LiKCl-600 with a *P6₃cm* space group for a sample prepared at 600 °C in a sealed glass ampoule using DCDA.[29] The strongest peak at ~26.8°, corresponding to a d spacing of ~3.3 Å, is assigned to the (002) reflection of2D cPTI nanosheets stacked in a graphitic fashion. This is further supported by transmission electron microscopy (TEM) images which show the graphite-like stacking (Figure 1b). The partial exfoliation of the graphite-like structure during washing with hot water gives rise to another strong peak at 28.4° (marked with an asterisk in Figure 1a), indicating a weak interplanar interaction between 2D cPTI layers.[29,30] Furthermore, the in-plane diffraction at 12.1°, corresponding to a d spacing of 7.3 Å, results from the trigonal voids spanned by triazine units, the intact ordering and stacking of which again confirm the successful thermal polycondensation of MCA into cPTI under the synthesis condition. We note a slight shift of the (002) peak to higher scattering angle. Replacement of N with O is probably responsible for such an interlayer contraction.[28]

Formation of oxygen containing cPTI is further supported by FT-IR spectroscopy. The FT-IR spectrum of PTI-MCA-LiKCl-550 shows the characteristic out-of-plane breathing mode of triazine at 803 cm^{-1} and the stretching mode of CN heterocyclic ring around 1100~1700 cm^{-1} (Figure 2a).[30] We attribute a small band at 1760 cm^{-1} and strong band at 1240 cm^{-1} to oxygen containing groups such as C=O or C-O.[21] The small band at 2170 cm^{-1} can be assigned to the surface nitrile group. A broad band around 3300 cm^{-1} indicates the presence of surface uncondensed amine (-NH- or -NH_2) or hydroxyl functional groups (-OH).

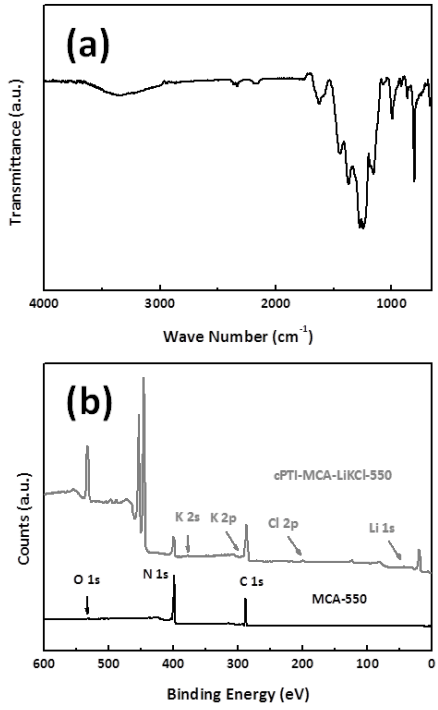

Figure 2. (a) FT-IR spectrum and (b) XPS survey spectrum of cPTI-MCA-LiKCl-550. XPS survey spectrum of MCA-550 prepared without the eutectic mixture was presented together for comparison.

Further insights into the chemical composition of cPTI-MCA-LiKCl-550 were given by elemental analysis (EA), X-ray photoelectron (XPS) and energy dispersive X-ray (EDX) spectroscopy studies. The H content that resulted from the surface uncondensed functional groups was estimated by EA to be 2.1 wt%. Although a similar degree of polycondensation (or C/N ratio calculated by EA) was expected from the H content, replacement of N with O resulted in a C/N ratio (0.76) for cPTI-MCA-LiKCl-550, which is much higher than that (0.64) of cPTI-DCDA-LiKCl-600.[30] Cyanuric acid seems to be incorporated into the cPTI framework in a manner similiar to that found in 4-AP or TAPI during ionothermal synthesis,[21,28] while the hydroxyl groups of cyanuric acid are known to easily decompose and thereby facilitate the polycondensation procedure in the absence of the eutectic mixtures.[26] A XPS survey scan indeed reveals the high O content in cPTI-MCA-LiKCl-550 compared to that in MCA-550 (Figure 2b). High resolution C 1s shows a new peak at 288.12 eV corresponding to C-O species in the cPTI framework, confirming that O is chemically bonded to a carbon atom of the triazine ring (Figure S1 in the Supporting Information).[31] The K and Cl contents were estimated from XPS to be about 2.3 and 1.3 wt%, respectively. The presence and homogeneous distribution of these, as well as C, N and O were also evidenced by EDX and elemental mapping analyses (Figure S2).

Scanning electron microscopy (SEM) images of cPTI-MCA-LiKCl-550 show a uniform rod-like morphology with a lateral size of ~300 nm and height of ~30 nm (Figure S3a). Nitrogen sorption analysis indicates a BET surface area of 58 m^2/g and a pore volume of 0.25 cm^3/g (Figure S3b). cPTI-MCA-LiKCl-550, with small particle size and high surface area compared to the bulk cPTI-DCDA-LiKCl-600, features textural properties appropriate for electrocatalytic applications in DSSCs as a CE catalyst.

Since the photovoltaic performance of DSSCs was poor when cPTI-MCA-LiKCl-550 was used alone as a CE catalyst (data not shown), two more additives that could be coated on the CE substrate were added to the catalyst solution. A conductive material, Super P® carbon black, was added to improve conductivity of the CE film according to a recent strategy.[32,33] In addition, poly(ethylene oxide) (PEO) of M_v ~5,000,000 was added as a sacrificial binder to make a homogenously dispersed solution and the resultant uniform CE film of cPTI-MCA-LiKCl-550/Super P. A drop-cast thin layer of this catalyst solution was dried at room temperature and annealed at 450 °C for 3 hrs under nitrogen to make ~25 µm thick CE films (Figure S4), which was also verified with a profilometer. Figure S5 shows the photovoltaic characteristics in case any of the three components is absent. In the absence of cPTI-MCA-LiKCl-550, the *PCE* is only 0.7% confirming that catalytic performance of the CE film mainly stems from cPTI-MCA-LiKCl-550. When Super P is not present, the fill factor (*FF*) is very low (0.28) due to high internal series resistance. Although the solution contains both cPTI-MCA-LiKCl-550 and Super P, it still has low *FF* (0.45) and poor *PCE* (3.9%) if PEO is absent. This shows that the role of PEO to microscopically blend g-CN and Super P is crucial in achieving high performance. The heating temperature during formation of CE films has significant influence on the *PCE* as well (Figure S6). By annealing the CE at higher temperatures, a higher *PCE* was obtained (5.2% for 300 °C, 6.4% for 400 °C, 7.8% for 450 °C).

Electrochemical impedence spectroscopy (EIS) measurements, which are the most convincing supporting analyses on the charge transfer process and catalytic activity,[34,35] were performed using a symmetric cell configuration to investigate the effect of the ratio change of the components. The dummy cells were prepared from four cPTI-MCA-LiKCl-550 catalyst solutions (designated as CC1, CC2, CC3, and CC4) with different content ratios of cPTI-MCA-LiKCl-550 and Super P (15:15, 20:10, 25:5, and 28:2, respectively) (Table 1). Each Nyquist plot consisted of two semicircles as shown in Figure 3, and they were fitted to the Randles circuit in the inset of Figure 3b. The left semicircle in the high frequency range represents the charge transfer resistance (R_{ct}) at the electrolyte/electrode interface and the corresponding capacitance (C_μ), and the right semicircle at low frequency can be assigned to the Nernst diffusion impedance (Z_N) of the redox species in the electrolyte.[34,35] The left semicircle becomes smaller with a higher ratio of cPTI-MCA-LiKCl-550 to Super P (CC1 to CC4), indicating that a lower R_{ct} can be obtained with a greater amount of cPTI-MCA-LiKCl-550 by the creation of more catalytic active sites. From a quantitative viewpoint, R_{ct} is calculated as half the value of the real component of impedance multiplied by the active area of each of the symmetric cells. The calculated R_{ct} values were 1.8, 1.5, and 0.5 Ω cm^2 for CC1, CC2, and CC3, respectively (Table 1). The Nyquist plot for CC4 did not provide an adequate fit to the equivalent Randles circuit, probably because the excess amount of cPTI-MCA-LiKCl-550 relative to the Super P concentration resulted in a less uniform CE film. It is noteworthy that the R_{ct} of CC3 was even lower than that of conventional Pt (1.1 Ω cm^2, in accordance with the normally reported values[36,37]), which implies that CC3 CEs can be more catalytically active than thermally platinized CEs. The right circle, however, became larger with higher content of cPTI-MCA-LiKCl-550 (CC1 to CC4). All the Z_N values in Table 1 were larger than that of Pt due to the thick CE films.

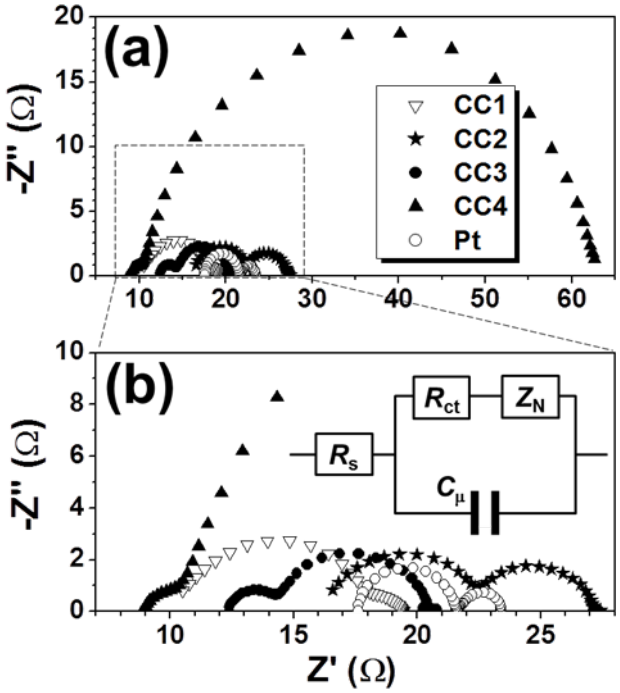

Figure 3. (a) Nyquist plot for the symmetrical cells, and (b) an expansion of the rectangle region of (a) and the equivalent circuit. The legend in (a) is for (b) as well.

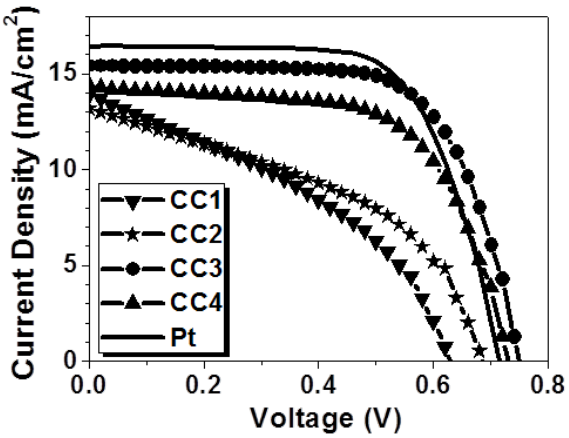

Figure 4. Characteristic J-V curves of DSSCs with cPTI-MCA-LiKCl-550 CEs and a Pt CE measured under simulated solar irradiation of AM 1.5 G (100 mW cm^{-2}).

cPTI	Super P	CE	V_{oc} (V)	J_{sc} (mA cm^{-2})	*FF*	*PCE* (%)	R_{ct} (Ω cm^2)	Z_N (Ω)
15	15	CC1	0.629	14.0	0.39	3.4	1.8	2.2
20	10	CC2	0.687	13.2	0.44	4.0	1.5	5.0
25	5	CC3	0.749	15.4	0.68	7.8	0.5	6.2
28	2	CC4	0.730	14.3	0.63	6.6	-	-
		Pt	0.715	16.4	0.67	7.9	1.1	1.9

Table 1. Summary of CE names, photovoltaic performances, and electrochemical impedance parameters. The numbers of cPTI and Super P represent their respective milligram weight dissolved in 1 mL catalyst solution.

Figure 4 and Table 1 show the photocurrent density-voltage (*J-V*) characteristics of the DSSCs using CEs prepared from cPTI-MCA-LiKCl-550 solutions and a conventional Pt CE. A lower R_{ct} leads to a higher *FF* by reducing the internal series resistance[38,39] for CC1, CC2, CC3 and Pt even if CC4 with the smallest left semicircle in the EIS analysis did not have the highest *FF* presumably due to its extremely high diffusion impedance. Also, DSSCs with high content of cPTI-MCA-LiKCl-550 (CC3 and CC4) showed higher V_{oc} than that of Pt, which was the result of a decrease in the overpotential for the triiodide reduction on the cPTI-MCA-LiKCl-550 CEs. However, all the J_{sc} values from the cPTI-MCA-LiKCl-550 CEs were lower than that of Pt. Among the four cPTI-MCA-LiKCl-550 electrodes, CC3 proved to be the most optimal with *FF* of 0.68, V_{oc} of 0.749 V, J_{sc} of 15.4 mA cm^{-2}, and *PCE* of 7.8% thereby showing a performance comparable to the standard DSSCs that use a Pt CE, a triiodide/iodide redox couple, an N719 dye, and FTO glass substrates. This result confirms that cPTI-MCA-LiKCl-550 with the help of a conductive material is a good candidate as an electrocatalyst in DSSCs. Also, when the long-term stability test of the solar cells was carried out under natural conditions, PCE maintained over 90% of initial values after 1000 h, confirming durability of the cPTI CEs.

Further improvement might be achieved in several ways. For example, J_{sc} may be increased by providing more catalytic active sites. When the CE materials do not maintain the required currents, the effective exchange current can be enhanced by increasing the CE surface area.[40] The drawback of a thick film and the resultant low surface area may be overcome by imparting greater porosity to the CE film. Doping cPTI-MCA-LiKCl-550 with other species or improving the coating technique to make a more uniform CE film could be another way to enhance the performance of the device.

In summary, oxygen-containing crystalline poly(triazine imide), cPTI-MCA-LiKCl-550, was prepared via a simple ionothermal method by using a MCA complex as a pre-organized, nitrogen-rich, and oxygen-containing precursor. When it was employed as a CE electrocatalyst in DSSCs, cPTI-MCA-LiKCl-550 gives a good *FF* of 0.68, V_{oc} of 0.749 V, and *PCE* of 7.8%. This high performance may be attributed to the low R_{ct} of cPTI-MCA-LiKCl-550 CEs and could be further improved by optimizing coating method, doping level, and surface area.

Acknowledgements

We gratefully acknowledge financial support from the National Science Foundation under Award No. DMR 0805148 and the University of California Lab Fees Research Program. This work was supported by the Institute for Collaborative Biotechnologies through grant W911NF-09-0001 from the U.S. Army Research Office. The content of the information does not necessarily reflect the position or the policy of the Government, and no official endorsement should be inferred. W.-r. L. is supported by the International Fulbright Science and Technology Award. The MRL Shared Experimental Facilities are supported by the MRSEC Program of the NSF under Award No. DMR 1121053; a member of the NSF-funded Materials Research Facilities Network (www.mrfn.org).

References

1 B. O'Regan and M. Grätzel, *Nature*, 1991, **353**, 737.
2 A. Hagfeldt, G. Boschloo, L. Sun, L. Kloo and H. Pettersson, *Chem. Rev.*, 2010, **110**, 6595.
3 Q. Tai and X.-Z. Zhao, *J. Mater. Chem. A*, 2014, **2**, 13207.
4 S. Ahmad, E. Guillén, L. Kavan, M. Grätzel and M. K. Nazeeruddin, *Energy Environ. Sci.*, 2013, **6**, 3439.
5 S. Yun, A. Hagfeldt and T. Ma, *Adv. Mater.*, 2014, **26**, 6210.
6 M. Wu and T. Ma, *J. Phys. Chem. C*, 2014, **118**, 16727.
7 H. Zheng, C. Y. Neo and J. Ouyang, *ACS Appl. Mater. Interfaces*, 2013, **5**, 6657.
8 H.-J. Ahn, I.-H. Kim, J.-C. Yoon, S.-I. Kim and J.-H. Jang, *Chem. Commun.*, 2014, **50**, 2412.
9 X. Wang, G. Sun, P. Routh, D.-H. Kim, W. Huang and P. Chen, *Chem. Soc. Rev.*, 2014, **43**, 7067.
10 J. E. Trancik, S. C. Barton and J. Hone, *Nano Lett.*, 2008, **8**, 982.
11 Y. Xue, J. Liu, H. Chen, R. Wang, D. Li, J. Qu and L. Dai, *Angew. Chem. Int. Ed.*, 2012, **51**, 12124.
12 S. Das, P. Sudhagar, V. Verma, D. Song, E. Ito, S. Y. Lee, Y. S. Kang and W. Choi, *Adv. Funct. Mater.*, 2011, **21**, 3729.

13 G. Algara-Siller, N. Severin, S. Y. Chong, T. Björkman, R. G. Palgrave, A. Laybourn, M. Antonietti, Y. Z. Khimyak, A. V. Krasheninnikov, J. P. Rabe, U. Kaiser, A. I. Cooper, A. Thomas and M. J. Bojdys, *Angew. Chem. Int. Ed*., 2014, **53**, 7450.
14 A. Thomas, A. Fischer, F. Goettmann, M. Antonietti, J.-O. Müller, R. Schlögl and J. M. Carlsson, *J. Mater. Chem*., 2008, **18**, 4893.
15 F. Goettmann, A. Fischer, M. Antonietti and A. Thomas, *Angew. Chem. Int. Ed*. 2006, **45**, 4467.
16 F. Goettmann, A. Thomas and M. Antonietti, *Angew. Chem. Int. Ed.*, 2007, **46**, 2717.
17 J. Liang, Y. Zheng, J. Chen, J. Liu, D. Hulicova-Jurcakova, M. Jaroniec and S. Z. Qiao, *Angew. Chem. Int. Ed*., 2012, **51**, 3892.
18 T. Y. Ma, S. Dai, M. Jaroniec and S. Z. Qiao, *Angew. Chem. Int. Ed*., 2014, **53**, 7281.
19 X. Wang, K. Maeda, A. Thomas, K. Takanabe, G. Xin, J. M. Carlsson, K. Domen and M. Antonietti, *Nat. Mater*., 2009, **8**, 76.
20 M. Shalom, S. Gimenez, F. Schipper, I. Herraiz-Cardona, J. Bisquert and M. Antonietti, *Angew. Chem. Int. Ed*., 2014, **53**, 3654.
21 K. Schwinghammer, B. Tuffy, M. B. Mesch, E. Wirnhier, C. Martineau, F. Taulelle, W. Schnick, J. Senker and B. V. Lotsch, *Angew. Chem. Int. Ed*., 2013, **52**, 2435.
22 M. J. Bojdys, J. O. Müller, M. Antonietti and A. Thomas, *Chem. Eur. J*., 2008, **14**, 8177.
23 N. Mansor, A. B. Jorge, F. Corà, C. Gibbs, R. Jervis, P. F. McMillan, X. Wang and D. J. L. Brett, *J. Phys. Chem. C*, 2014, **118**, 6831.
24 E. Olsen, G. Hagen and S. E. Lindquist, *Sol. Energ. Mat. Sol. Cells*, 2000, **63**, 267.
25 Y. Gao, L. Chu, M. Wu, L. Wang, W. Guo and T. Ma, *J. Photochem. Photobiol. A*, 2012, **245**, 66.
26 Y. S. Jun, E. Z. Lee, X. Wang, W. H. Hong, G. D. Stucky and A. Thomas, *Adv. Funct. Mater*., 2013, **23**, 3661.
27 J. D. Roy-Mayhew, D. J. Bozym, C. Punckt and I. A. Aksay, *ACS Nano*, 2010, **4**, 6203.
28 M. K. Bhunia, K. Yamauchi and K. Takanabe, *Angew. Chem. Int. Ed.*, 2014, **53**, 11001.
29 Y. Ham, K. Maeda, D. Cha, K. Takanabe and K. Domen, *Chem. Asian J.*, 2013, **8**, 218.
30 K. Schwinghammer, M. B. Mesch, V. Duppel, C. Ziegler, J. Senker and B. V. Lotsch, *J. Am. Chem. Soc*., 2014, **136**, 1730.
31 Z.-F. Huang, J. Song, L. Pan, Z. Wang, X. Zhang, J.-J. Zou, W. Mi, X. Zhang and L. Wang, *Nano Energy*, 2015, **12**, 646.
32 M. Wu, X. Lin, Y. Wang, L. Wang, W. Guo, D. Qi, X. Peng, A. Hagfeldt, M. Grätzel and T. Ma, *J. Am. Chem. Soc*., 2012, **134**, 3419.
33 G. R. Li, F. Wang, Q. W. Jiang, X. P. Gao and P. W. Shen, *Angew. Chem. Int. Ed*., 2010, **49**, 3653.
34 A. Hauch and A. Georg, *Electrochim. Acta*, 2001, **46**, 3457.
35 M. Wang, A. M. Anghel, B. Marsan, N. L. C. Ha, N. Pootrakulchote, S. M. Zakeeruddin and M. Grätzel, *J. Am. Chem. Soc.*, 2009, **131**, 15976.
36 J. D. Roy-Mayhew and I. A. Aksay, *Chem. Rev*., 2014, **114**, 6323.
37 K. Yu, Z. Wen, H. Pu, G. Lu, Z. Bo, H. Kim, Y. Qian, E. Andrew, S. Mao and J. Chen, *J. Mater. Chem*. A, 2013, **1**, 188.
38 S. Hou, X. Cai, H. Wu, X. Yu, M. Peng, K. Yan and D. Zou, *Energy Environ. Sci*., 2013, **6**, 3356.
39 X. Zheng, J. Deng, N. Wang, D. Deng, W. H. Zhang, X. Bao and C. Li, *Angew. Chem. Int. Ed*., 2014, **53**, 7023.
40 N. Papageorgiou, *Coord. Chem. Rev*., 2004, **248**, 1421.